Integral Transforms and Special Functions
Vol. 17, No. 9, September 2006, 637–652

Taylor & Francis
Taylor & Francis Group

Computation of the generalized Mittag-Leffler function and its inverse in the complex plane

R. HILFER*†‡ and H. J. SEYBOLD†

†Institut für Computerphysik, Universität Stuttgart, 70569 Stuttgart, Germany
‡Institut für Physik, Universität Mainz, 55099 Mainz, Germany

(Received 21 March 2005)

The generalized Mittag-Leffler function $\mathrm{E}_{\alpha,\beta}(z)$ has been studied for arbitrary complex argument $z \in \mathbb{C}$ and parameters $\alpha \in \mathbb{R}^+$ and $\beta \in \mathbb{R}$. This function plays a fundamental role in the theory of fractional differential equations and numerous applications in physics. The Mittag-Leffler function interpolates smoothly between exponential and algebraic functional behaviour. A numerical algorithm for its evaluation has been developed. The algorithm is based on integral representations and exponential asymptotics. Results of extensive numerical calculations for $\mathrm{E}_{\alpha,\beta}(z)$ in the complex z-plane are reported here. We find that all complex zeros emerge from the point $z = 1$ for small α. They diverge towards $-\infty + (2k-1)\pi\mathrm{i}$ for $\alpha \to 1^-$ and towards $-\infty + 2k\pi\mathrm{i}$ for $\alpha \to 1^+$ ($k \in \mathbb{Z}$). All the complex zeros collapse pairwise onto the negative real axis for $\alpha \to 2$. We introduce and study also the inverse generalized Mittag-Leffler function $\mathrm{L}_{\alpha,\beta}(z)$ defined as the solution of the equation $\mathrm{L}_{\alpha,\beta}(\mathrm{E}_{\alpha,\beta}(z)) = z$. We determine its principal branch numerically.

Keywords: Special functions of mathematical physics; Fractional calculus; Generalized Mittag-Leffler functions; Numerical algorithms

PACS: 02.30.Gp; 02.60.Gf

1. Introduction

A special function of growing importance is the generalized Mittag-Leffler function defined by the power series [1, p. 210]

$$\mathrm{E}_{\alpha,\beta}(z) = \sum_{k=0}^{\infty} \frac{z^k}{\Gamma(\alpha k + \beta)} \tag{1}$$

for complex argument $z \in \mathbb{C}$ and parameters $\alpha, \beta \in \mathbb{C}$ with $\mathrm{Re}\,\alpha > 0$. Despite the fact that $\mathrm{E}_{\alpha,\beta}$ was introduced roughly 100 years ago [2–7], its mapping properties in the complex plane are largely unknown.

Mittag-Leffler functions are important in mathematical as well as in theoretical and applied physics [8–17]. A primary reason for the recent surge of interest in these functions is their

*Corresponding author. ICP, Univ. Stuttgart, Pfaffenwaldring 27, 70569 Stuttgart

Integral Transforms and Special Functions
ISSN 1065-2469 print/ISSN 1476-8291 online © 2006 Taylor & Francis
http://www.tandf.co.uk/journals
DOI: 10.1080/10652460600725341

appearance when solving the fractional differential equation

$$\mathrm{D}_{a+}^{\alpha,\gamma} f(x) = \lambda f(x) \quad 0 < \alpha \leq 1, \quad 0 \leq \gamma \leq 1, \quad \lambda \in \mathbb{R} \tag{2}$$

where $\mathrm{D}_{a+}^{\alpha,\gamma}$ is a fractional derivative of order α and type γ with lower limit a [17]. In equation (2), the symbol $\mathrm{D}_{a+}^{\alpha,\gamma}$ stands for [17, p. 115]

$$\mathrm{D}_{a+}^{\alpha,\gamma} f(x) = \left[\mathrm{I}_{a+}^{\gamma(1-\alpha)} \frac{\mathrm{d}}{\mathrm{d}x} \mathrm{I}_{a+}^{(1-\gamma)(1-\alpha)} f \right](x) \quad 0 < \alpha \leq 1, \quad 0 \leq \gamma \leq 1 \tag{3}$$

for the functions for which the expression on the right-hand side exists. Of course, the notation $\mathrm{I}_{a+}^{\alpha} f(x)$ stands for the right sided fractional Riemann–Liouville integral of order $\alpha \in \mathbb{R}^+$ defined by

$$\mathrm{I}_{a+}^{\alpha} f(x) = \frac{1}{\Gamma(\alpha)} \int_a^x (x-t)^{\alpha-1} f(t) \mathrm{d}t \quad \text{with} \quad a \leq x \leq b, \quad \alpha \in \mathbb{R}^+ \tag{4}$$

for locally integrable functions $f \in L^1[a, b]$. Recall from ref. [17, p. 115] that equation (2) is solved for $a = 0$ by

$$f(x) = x^{(1-\gamma)(\alpha-1)} \mathrm{E}_{\alpha,\alpha+\gamma(1-\alpha)}(\lambda x^{\alpha}), \tag{5}$$

where $\mathrm{E}_{\alpha,\beta}(z)$ is the generalized Mittag-Leffler function. Equation (2) shows that the Mittag-Leffler function plays the same role for fractional calculus that the exponential function plays for conventional calculus. Mittag-Leffler functions and fractional calculus have in recent years become a powerful tool to investigate anomalous dynamics and strange kinetics [12, 17–19].

Despite the growing importance of $\mathrm{E}_{\alpha,\beta}(z)$ in physics and despite a wealth of analytical information about $\mathrm{E}_{\alpha,\beta}(z)$, its behaviour as a holomorphic function and dependence upon the parameters are largely unexplored, because there seem to be no numerical algorithms available to compute the function accurately for all α, β, z. Easy numerical evaluation and a thorough understanding of $\mathrm{E}_{\alpha,\beta}(z)$ as a function of α, β, z is, however, a key prerequisite for extending its applications to other disciplines. It is therefore desirable to explore the behaviour of $\mathrm{E}_{\alpha,\beta}(z)$ for large sets of the parameters α and β and the complex argument z.

Given this objective, the present article reports a newly developed numerical algorithm as well as extensive computations for the generalized Mittag-Leffler function. Little will be said in this article about the algorithm apart from giving its complete definition. While this work was in progress a simpler algorithm appeared in ref. [20]. A detailed comparison between the two algorithms can be found in ref. [21]. One should note that the algorithm works not only on the real axis, but in the full complex plane. Rather than discussing the details of the algorithm, we concentrate here on exploring the functional behaviour of $\mathrm{E}_{\alpha,\beta}(z)$. In particular, we study its complex zeros and illustrate its behaviour as an entire function. As an example, we find that the zeros of $\mathrm{E}_{\alpha,\beta}$ coalesce to form a simple pole in the limit $\alpha \to 0$. Moreover, the zeros diverge in a complicated fashion to $-\infty$ as α approaches unity from above as well as from below.

2. Method of calculation

2.1 *Recursion relation*

In the rest of this article, α and β are real numbers with $\alpha > 0$. Calculating $\mathrm{E}_{\alpha,\beta}(z)$ for the case $\alpha > 1$ can be reduced to the case $0 < \alpha \leq 1$ by virtue of the recursion relation [1, 22]

$$\mathrm{E}_{\alpha,\beta}(z) = \frac{1}{2m+1} \sum_{h=-m}^{m} \mathrm{E}_{\alpha/(2m+1),\beta}(z^{1/(2m+1)} \mathrm{e}^{2\pi \mathrm{i} h/(2m+1)}) \tag{6}$$

valid for all $\beta \in \mathbb{R}$, $z \in \mathbb{C}$ where $m = [(\alpha - 1)/2] + 1$. Here $[x]$ denotes the largest integer smaller than x. Because of the recursion we consider only the case $0 < \alpha \leq 1$ in the rest of this section.

2.2 *Regions*

For $0 < \alpha \leq 1$ the complex z-plane is partitioned into four regions $\mathbb{G}_0$, $\mathbb{G}_1$, $\mathbb{G}_2$ and $\mathbb{G}_3$. In each region, a different method is used for the calculation of the Mittag-Leffler function. The central region

$$\mathbb{G}_0 = \overline{\mathbb{D}(r_0)} = \{z \in \mathbb{C}\colon |z| \leq r_0\} \tag{7}$$

is the closure of the open disk $\mathbb{D}(r_0) = \{z \in \mathbb{C}\colon |z| < r_0\}$ of radius $r_0 < 1$ centered at the origin. In our numerical calculations we have chosen $r_0 = 0.9$ throughout. The regions $\mathbb{G}_1$, $\mathbb{G}_2$ are defined by

$$\mathbb{G}_1 = \mathbb{W}^+\left(\frac{5\pi\alpha}{6}\right) \setminus \mathbb{G}_0 \tag{8}$$

$$\mathbb{G}_2 = \mathbb{C} \setminus (\mathbb{G}_1 \cup \mathbb{G}_0) \tag{9}$$

where

$$\mathbb{W}^+(\phi) = \{z \in \mathbb{C}\colon |\arg(z)| < \phi\} \tag{10}$$

is the open wedge with opening angle ϕ, $(0 < \phi < \pi)$. For future reference we define also the (left) wedge

$$\mathbb{W}^-(\phi) = \{z \in \mathbb{C}\colon \phi < |\arg(z)| \leq \pi\} \tag{11}$$

Finally, the region $\mathbb{G}_3$ is defined as

$$\mathbb{G}_3 = \mathbb{C} \setminus \mathbb{D}(r_1) = \{z \in \mathbb{C}\colon |z| > r_1\} \tag{12}$$

where $r_1 > r_0$ will be defined below.

2.3 *Taylor series*

For $z \in \mathbb{G}_0$, *i.e.* for the central disk region (with $r_0 = 0.9$), the Mittag-Leffler function is computed from truncating its Taylor series (1). For a given $z \in \mathbb{G}_0$ and accuracy ϵ, we choose

N such that

$$\left| \mathrm{E}_{\alpha,\beta}(z) - \sum_{k=0}^{N} \frac{z^k}{\Gamma(\alpha k + \beta)} \right| \leq \epsilon \tag{13}$$

holds. The dependence of N on the accuracy ϵ and the other parameters is found as

$$N \geq \max \left\{ \left[\frac{2-\beta}{\alpha} \right] + 1, \left[\frac{\ln(\epsilon(1-|z|))}{\ln(|z|)} \right] + 1 \right\}. \tag{14}$$

2.4 *Integral representations*

We start from the basic integral representation [1, p. 210]

$$\mathrm{E}_{\alpha,\beta}(z) = \frac{1}{2\pi \mathrm{i}} \int_{\mathcal{C}} \frac{y^{\alpha-\beta} \mathrm{e}^{y}}{y^{\alpha} - z} \mathrm{d}y \tag{15}$$

where the path of integration $\mathcal{C}$ in the complex plane starts and ends at $-\infty$ and encircles the circular disc $|y| \leq |z|^{1/\alpha}$ in the positive sense. When this integral is evaluated, several cases arise. For $z \in \mathbb{G}_1$, we distinguish the cases $\beta \leq 1$ and $\beta > 1$ and compute the Mittag-Leffler function from the integral representations [23]

$$\mathrm{E}_{\alpha,\beta}(z) = A(z;\alpha,\beta,0) + \int_0^{\infty} B(r;\alpha,\beta,z,\pi\alpha)\mathrm{d}r, \quad \beta \leq 1 \tag{16}$$

$$\mathrm{E}_{\alpha,\beta}(z) = A(z;\alpha,\beta,0) + \int_{1/2}^{\infty} B(r;\alpha,\beta,z,\pi\alpha)\mathrm{d}r + \int_{-\pi\alpha}^{\pi\alpha} C\left(\varphi;\alpha,\beta,z,\frac{1}{2}\right)\mathrm{d}\varphi, \quad \beta > 1 \tag{17}$$

where

$$A(z;\alpha,\beta,x) = \frac{1}{\alpha} z^{(1-\beta)/\alpha} \exp\left[z^{1/\alpha} \cos\left(\frac{x}{\alpha}\right) \right] \tag{18}$$

$$B(r;\alpha,\beta,z,\phi) = \frac{1}{\pi} A(r;\alpha,\beta,\phi) \frac{r \sin[\omega(r,\phi,\alpha,\beta) - \phi] - z \sin[\omega(r,\phi,\alpha,\beta)]}{r^2 - 2rz\cos\phi + z^2} \tag{19}$$

$$C(\varphi;\alpha,\beta,z,\rho) = \frac{\rho}{2\pi} A(\rho;\alpha,\beta,\varphi) \frac{\cos[\omega(\rho,\varphi,\alpha,\beta)] + \mathrm{i}\sin[\omega(\rho,\varphi,\alpha,\beta)]}{\rho(\cos\varphi + \mathrm{i}\sin\varphi) - z} \tag{20}$$

$$\omega(x,y,\alpha,\beta) = x^{1/\alpha} \sin\left(\frac{y}{\alpha}\right) + y\left(1 + \frac{1-\beta}{\alpha}\right). \tag{21}$$

For $z \in \mathbb{G}_2$, the integral representations read

$$\mathrm{E}_{\alpha,\beta}(z) = \int_0^{\infty} B\left(r;\alpha,\beta,z,\frac{2\pi\alpha}{3}\right)\mathrm{d}r, \quad \beta \leq 1 \tag{22}$$

$$\mathrm{E}_{\alpha,\beta}(z) = \int_{1/2}^{\infty} B\left(r;\alpha,\beta,z,\frac{2\pi\alpha}{3}\right)\mathrm{d}r + \int_{-2\pi\alpha/3}^{2\pi\alpha/3} C\left(\varphi;\alpha,\beta,z,\frac{1}{2}\right)\mathrm{d}\varphi, \quad \beta > 1 \tag{23}$$

where the integrands have been defined in equations (18)–(21).

The integrand $C(\varphi; \alpha, \beta, z, \rho)$ is oscillatory but bounded over the integration interval. Thus, the integrals over C can be evaluated numerically using any appropriate quadrature formula. We use a robust Gauss–Lobatto quadrature.

The integrals over $B(r; \alpha, \beta, z, \phi)$ involve infinite intervals. For a given $z \in \mathbb{G}_1$ (respectively $z \in \mathbb{G}_2$) and the accuracy ϵ, we approximate the integrals by truncation. The error

$$\left| \int_{R_{\max}}^{\infty} B(r; \alpha, \beta, z, \phi) \mathrm{d}r \right| < \epsilon \tag{24}$$

depends on the truncation point $R_{\max}$. For $\phi = \pi\alpha$ we find

$$R_{\max} \geq \begin{cases} \max\left\{1,\ 2|z|,\ \left(-\ln \dfrac{\pi\epsilon}{6}\right)^{\alpha}\right\} & \beta \geq 0 \\ \max\left\{(|\beta|+1)^{\alpha},\ 2|z|,\ \left(-2\ln\left(\dfrac{\pi\epsilon}{6(|\beta|+2)(2|\beta|)^{|\beta|}}\right)\right)^{\alpha}\right\} & \beta < 0. \end{cases} \tag{25}$$

while for $\phi = 2\pi\alpha/3$ we have

$$R_{\max} \geq \begin{cases} \max\left\{2^{\alpha},\ 2|z|,\ \left(-2\ln \dfrac{\pi 2^{\beta}\epsilon}{12}\right)^{\alpha}\right\} & \beta \geq 0 \\ \max\left\{[2(|\beta|+1)]^{\alpha},\ 2|z|,\ \left[-4\ln \dfrac{\pi 2^{\beta}\epsilon}{12(|\beta|+2)(4|\beta|)^{|\beta|}}\right]^{\alpha}\right\} & \beta < 0. \end{cases} \tag{26}$$

2.5 *Exponential asymptotics*

The asymptotic expansions given in equations (21) and (22) on page 210 in ref. [1] indicate that the Mittag-Leffler function exhibits a Stokes phenomenon. The Stokes lines are the rays $\arg(z) = \pm\alpha\pi$, and it was recently shown in ref. [24] that a Berry-type smoothing applies. The exponentially improved asymptotic expansions will be used here for computing $\mathrm{E}_{\alpha,\beta}(z)$ for $z \in \mathbb{G}_3$. More precisely, for $0 < \alpha < 1$ we use the following exponentially improved uniform asymptotic expansions [24]:

$$\mathrm{E}_{\alpha,\beta}(z) = -\sum_{k=1}^{M} \frac{z^{-k}}{\Gamma(\beta - \alpha k)} + O(|z|^{(1/2-\beta)/\alpha} \mathrm{e}^{-|z|^{1/\alpha}}) \tag{27}$$

for $z \in \mathbb{G}_3 \cap \mathbb{W}^{-}(\alpha\pi + \delta)$

$$\mathrm{E}_{\alpha,\beta}(z) = \frac{1}{\alpha} z^{(1-\beta)/\alpha} \mathrm{e}^{z^{1/\alpha}} - \sum_{k=1}^{M} \frac{z^{-k}}{\Gamma(\beta - \alpha k)} + O(|z|^{(1/2-\beta)/\alpha} \mathrm{e}^{-|z|^{1/\alpha}}) \tag{28}$$

for $z \in \mathbb{G}_3 \cap \mathbb{W}^{+}(\alpha\pi - \delta)$,

$$\mathrm{E}_{\alpha,\beta}(z) = \frac{1}{2\alpha} z^{(1-\beta)/\alpha} \mathrm{e}^{z^{1/\alpha}} \operatorname{erfc}\left(\left(\frac{c^3}{36} - \frac{\mathrm{i}c^2}{6} - c\right)\sqrt{|z|^{1/\alpha}/2}\right) - \sum_{k=1}^{M} \frac{z^{-k}}{\Gamma(\beta - \alpha k)} + O(|z|^{(1/2-\beta)/\alpha} \mathrm{e}^{-|z|^{1/\alpha}}) \tag{29}$$

for $z \in \mathbb{G}_3$ with $-\alpha\pi - \delta \le \arg(z) \le -\alpha\pi + \delta$ and $c = \arg(z^{1/\alpha}) + \pi$, and

$$\mathrm{E}_{\alpha,\beta}(z) = \frac{1}{2\alpha} z^{(1-\beta)/\alpha} \mathrm{e}^{z^{1/\alpha}} \operatorname{erfc}\left(\left(c + \frac{\mathrm{i}c^2}{6} - \frac{c^3}{36}\right)\sqrt{\frac{|z|^{1/\alpha}}{2}}\right) - \sum_{k=1}^{M} \frac{z^{-k}}{\Gamma(\beta - \alpha k)} + O\left(|z|^{(1/2-\beta)/\alpha} \mathrm{e}^{-|z|^{1/\alpha}}\right) \tag{30}$$

for $z \in \mathbb{G}_3$ with $\alpha\pi - \delta \le \arg(z) \le \alpha\pi + \delta$ and $c = \arg(z^{1/\alpha}) - \pi$. Here $\delta > 0$ is a small number; in practice, we use $\delta = 0.01$. In equations (29) and (30)

$$\operatorname{erfc}(z) = \frac{2}{\sqrt{\pi}} \int_z^\infty \mathrm{e}^{y^2/2}\, \mathrm{d}y \tag{31}$$

denotes the complex complementary error function. Note the difference between equations (27)–(30) and the expansions in ref. [1, p. 210]. We take

$$M = \min\left\{50, \left[\frac{|z|^{1/\alpha}}{\alpha}\right]\right\} \tag{32}$$

to truncate the asymptotic series. Choosing for ϵ, the machine precision, we fix the radius r_1 in $\mathbb{G}_3$ at

$$r_1 = \frac{1}{[\epsilon\Gamma(\beta - \alpha M)]^{1/M}}. \tag{33}$$

The remainder estimates in equations (27)–(30) are only valid for a value of M that is chosen in an optimal sense, as in equations (32) and (33).

3. Results

In this section, we present the results of the extensive numerical calculations using an algorithm that is based on the error estimates developed earlier. Our results give a comprehensive picture of the behaviour of $\mathrm{E}_{\alpha,\beta}(z)$ in the complex z-plane for all values of the parameters $\alpha > 0$, $\beta \in \mathbb{R}$.

3.1 *Complex zeros*

Contrary to the exponential function, the Mittag-Leffler functions exhibit complex zeros denoted as z^0. The complex zeros were studied by Wiman [7] who found the asymptotic curve along which the zeros are located for $0 < \alpha < 2$ and showed that they fall on the negative real axis for all $\alpha \ge 2$. For real α and β, these zeros come in complex conjugate pairs. The pairs are denoted as $z_k^0(\alpha)$ with integers $k \in \mathbb{Z}$ where $k > 0$ (respectively $k \le 0$) labels the zeros in the upper (respectively lower) half plane. Figure 1 shows the lines that the complex zeros $z_k^0(\alpha)$, $k = -5, \ldots, 6$ of $\mathrm{E}_{\alpha,1}(z)$ trace out as functions of α for $0.1 \le \alpha \le 0.99995$. Figure 1 gives strong numerical evidence that the distance between the zeros diminishes as $\alpha \to 0$. Moreover, all the zeros approach the point $z = 1$ as $\alpha \to 0$. This fact seems to have been overlooked until now. Of course, for every fixed $\alpha > 0$ the point $z = 1$ is neither a zero nor an accumulation point of the zeros, because the zeros of an entire function must remain isolated. The numerical evidence is confirmed analytically.

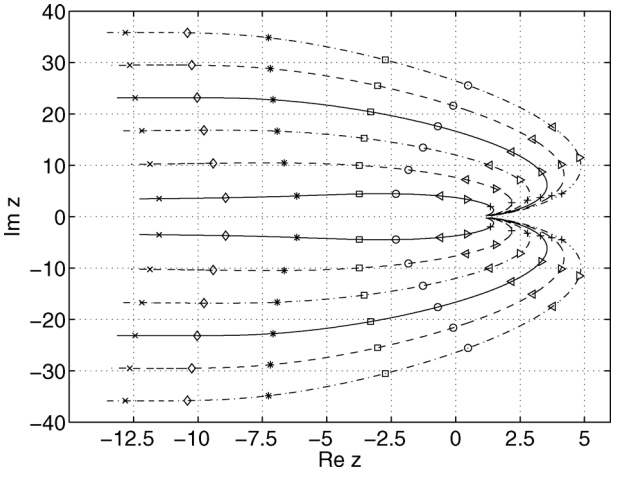

Figure 1. The lines trace out the locus of complex zeros $z_k^0(\alpha)$ as functions of α for $k = -5, \ldots, 6$ for the Mittag-Leffler function $\mathrm{E}_{\alpha,1}(z)$ in the range $0.1 \le \alpha \le 0.99995$. The line styles consecutively label $k = 0$, 1 (solid) $k = -1$, 2 (dashed) $k = -2$, 3 (dash-dotted), $k = -3$, 4 (solid) $k = -4$, 5 (dashed) and $k = -5$, 6 (dash-dotted). The symbols mark $\alpha = 0.5$ (plus), $\alpha = 0.7$ (triangle right), $\alpha = 0.8$ (triangle left), $\alpha = 0.9$ (circle), $\alpha = 0.95$ (square), $\alpha = 0.99$ (asterisk), $\alpha = 0.999$ (diamond), and $\alpha = 0.9999$ (cross).

THEOREM 3.1 *The zeros* $z_k^0(\alpha)$ *of* $\mathrm{E}_{\alpha,1}(z)$ *obey*

$$\lim_{\alpha \to 0} z_k^0(\alpha) = 1 \tag{34}$$

for all $k \in \mathbb{Z}$.

For the proof we note that Wiman showed [7, p. 226]

$$\lim_{k \to \infty} \arg z_{\pm k}^0(\alpha) = \pm \frac{\alpha \pi}{2} \tag{35}$$

and further that the number of zeros with $z_k^0 < r$ is given by $r^{1/\alpha}/\pi - 1 + (\alpha/2)$ [7, p. 228]. From this follows that

$$\left(1 - \frac{\alpha}{2}\right)^{\alpha} \pi^{\alpha} < |z_k^0(\alpha)| < \left(2k + 1 - \frac{\alpha}{2}\right)^{\alpha} \pi^{\alpha} \tag{36}$$

for all $k \in \mathbb{Z}$. Taking the limit $\alpha \to 0$ in equations (35) and (36) gives $|z_k(0)| = 1$ and $\arg z_k(0) = 0$ for all $k \in \mathbb{Z}$. The theorem states that in the limit $\alpha \to 0$ all the zeros collapse into a singularity at $z = 1$.

Next we turn to the limit $\alpha \to 1$. Of course for $\alpha = 1$ we have $\mathrm{E}_{1,1}(z) = \exp z$, which is free from zeros. Figure 1 shows that this is indeed the case because, as $\alpha \to 1$, the zeros approach $-\infty$ along the straight lines parallel to the negative real axis.

THEOREM 3.2 *Let* $\epsilon > 0$. *Then the zeros* $z_k^0(\alpha)$ *of* $\mathrm{E}_{\alpha,1}(z)$ *obey*

$$\lim_{\epsilon \to 0} \operatorname{Im} z_k^0(1 - \epsilon) = (2k - 1)\pi \tag{37}$$

$$\lim_{\epsilon \to 0} \operatorname{Im} z_k^0(1 + \epsilon) = 2k\pi \tag{38}$$

for all $k \in \mathbb{Z}$.

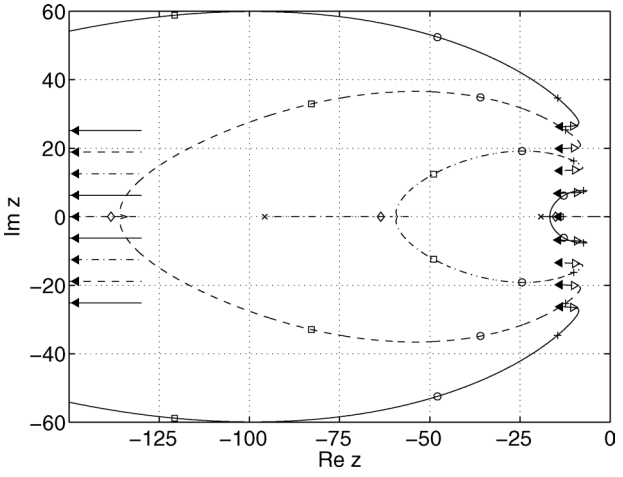

Figure 2. Locus of complex zeros $z_k^0(\alpha)$ as functions of α for $k = \pm 1, \pm 2, \pm 3, \pm 4$ for the Mittag-Leffler function $\mathrm{E}_{\alpha,1}(z)$ in the range $1.00001 \leq \alpha \leq 1.9$. The line styles consecutively label $k = \pm 1$ (solid) $k = \pm 2$ (dashed) $k = \pm 3$ (dash-dotted), $k = \pm 4$ (solid). The symbols mark $\alpha = 1.00001$ (triangle left filled) $\alpha = 1.001$ (triangle right) $\alpha = 1.1$ (plus) $\alpha = 1.3$ (circle) $\alpha = 1.5$ (square), and $\alpha = 1.7$ (diamond) $\alpha = 1.9$ (cross). The arrows on the left indicate the asymptotic locations $z_k^0(1) = 2k\pi$ in the limit $\alpha \to 1$ from above.

The theorem shows that the phase switches as α crosses the value $\alpha = 1$ in the sense that minima (valleys) and maxima (hills) of the Mittag-Leffler function are exchanged (see also figures 7 and 8).

The location of zeros as function of α for the case $1 < \alpha < 2$ is illustrated in figure 2. Note that with increasing α more and more pairs of zeros collapse onto the negative real axis. The collapse appears to happen in a continuous manner (see also figures 9 and 10). It is interesting to note that after two conjugate zeros merge to become a single zero on the negative real axis, this merged zero first moves to the right towards zero, and only afterwards starts to move left towards $-\infty$. This effect can also be seen in figure 2. For $\alpha = 2$, the zeros $-(k - (1/2))^2\pi^2$ all fall on the negative real axis, as can be seen in figure 11. For $\alpha > 2$, all the zeros lie on the negative real axis.

3.2 *Contour lines*

Next we present contour plots for $\mathrm{Re}\,\mathrm{E}_{\alpha,\beta}(z)$. We use the notation

$$\mathcal{C}^{\mathrm{Re}}_{\alpha,\beta}(v) = \{z \in \mathbb{C}\colon \mathrm{Re}\,\mathrm{E}_{\alpha,\beta}(z) = v\} \tag{39}$$

$$\mathcal{C}^{\mathrm{Im}}_{\alpha,\beta}(v) = \{z \in \mathbb{C}\colon \mathrm{Im}\,\mathrm{E}_{\alpha,\beta}(z) = v\} \tag{40}$$

for the contour lines of the real and the imaginary part. The region $\{z \in \mathbb{C}\colon \mathrm{Re}\,\mathrm{E}_{\alpha,\beta}(z) > 1\}$ will be coloured white. The region $\{z \in \mathbb{C}\colon \mathrm{Re}\,\mathrm{E}_{\alpha,\beta}(z) < -1\}$ will be coloured black. The region $\{z \in \mathbb{C}\colon 0 \leq \mathrm{Re}\,\mathrm{E}_{\alpha,\beta}(z) \leq 1\}$ is light grey. The region $\{z \in \mathbb{C}\colon -1 \leq \mathrm{Re}\,\mathrm{E}_{\alpha,\beta}(z) \leq 0\}$ is dark grey. Thus the contour line $\mathcal{C}^{\mathrm{Re}}_{\alpha,\beta}(0)$ separates light grey from dark grey, the contour $\mathcal{C}^{\mathrm{Re}}_{\alpha,\beta}(1)$ separates white from light grey, and $\mathcal{C}^{\mathrm{Re}}_{\alpha,\beta}(-1)$ dark grey from black. Because $\mathrm{Re}\,\mathrm{E}_{\alpha,\beta}(z)$ is continuous, there exists in all figures light and dark grey regions between white and black regions even if the grey regions cannot be discerned on a figure.

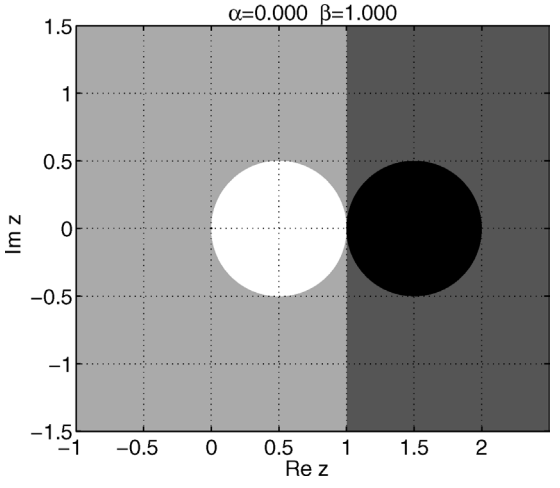

Figure 3. Contour plot for $\operatorname{Re} \mathrm{E}_{0,1}(z)$. The region $\{z \in \mathbb{C} : \operatorname{Re} \mathrm{E}_{\alpha,\beta}(z) > 1\}$ is white, $\{z \in \mathbb{C} : \operatorname{Re} \mathrm{E}_{\alpha,\beta}(z) < -1\}$ is black, $\{z \in \mathbb{C} : 0 \leq \operatorname{Re} \mathrm{E}_{\alpha,\beta}(z) \leq 1\}$ is light grey, and $\{z \in \mathbb{C} : -1 \leq \operatorname{Re} \mathrm{E}_{\alpha,\beta}(z) \leq 0\}$ is dark grey.

We begin our discussion with the case $\alpha \to 0$. Setting $\alpha = 0$, the series (1) defines the function

$$\mathrm{E}_{0,\beta}(z) = \frac{1}{\Gamma(\beta)(1-z)} \tag{41}$$

for all $|z| < 1$. This function is not entire, but can be analytically continued to all of $\mathbb{C} \setminus \{1\}$, and has then a simple pole at $z = 1$ for all β. In figure 3 we show the contour plot for the case $\alpha = 0$, $\beta = 1$. The contour line $\mathcal{C}^{\mathrm{Re}}_{0,1}(0)$ is the straight line $\operatorname{Re} z = 1$ separating the left and the right half plane. The contour line $\mathcal{C}^{\mathrm{Re}}_{0,1}(1)$ is the boundary circle of the white disc on the left, while the contour line $\mathcal{C}^{\mathrm{Re}}_{0,1}(-1)$ is the boundary of the black disc on the right.

Having discussed the case $\alpha = 0$, we turn to the case $\alpha > 0$ and note that the limit $\alpha \to 0$ is not continuous. For $\alpha > 0$ the Mittag-Leffler function is an entire function. As an example, we show the contour plot for $\alpha = 0.2$, $\beta = 1$ in figure 4. The central white circular lobe extending

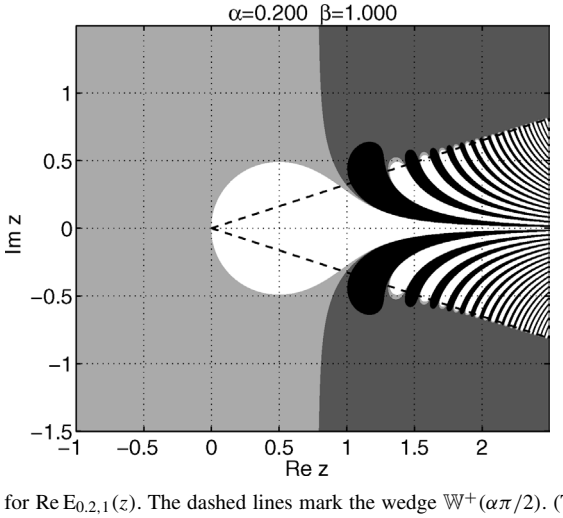

Figure 4. Contour plot for $\operatorname{Re} \mathrm{E}_{0.2,1}(z)$. The dashed lines mark the wedge $\mathbb{W}^{+}(\alpha\pi/2)$. (The grey level coding is the same as in figure 3.)

to the origin appears to be a remnant of the white disc in figure 3. They evolve continuously from each other upon changing α between 0 and 0.2. It seems as if the singularity at $z = 1$ for $\alpha = 0$ had moved along the real axis through the black circle to ∞, thereby producing an infinite number of the secondary white and black lobes (or fingers) confined to a wedge-shaped region with an opening angle $\alpha\pi/2$.

The behaviour of $\mathrm{E}_{\alpha,\beta}(z)$ for $0 < \alpha < 2$ is generally dominated by the wedge $\mathbb{W}^+(\alpha\pi/2)$ indicated by dashed lines in figure 4. For $z \in \mathbb{W}^+(\alpha\pi/2)$ the Mittag-Leffler function grows to infinity as $|z| \to \infty$. Inside this wedge the function oscillates as a function of $\mathrm{Im}\, z$. For $z \in \mathbb{W}^-(\alpha\pi/2)$ the function decays to zero as $|z| \to \infty$. Along the delimiting rays, *i.e.* for $\arg(z) = \pm\alpha\pi/2$, the function approaches $1/\alpha$ in an oscillatory fashion.

The oscillations inside the wedge are seen as black and white lobes (or fingers) in figure 4. Each white finger is surrounded by a light grey region. Near the tip of the light grey region surrounding a white finger lie complex zeros of the Mittag-Leffler function. The real part $\mathrm{Re}\, \mathrm{E}_{\alpha,\beta}(z)$ is symmetric with respect to the real axis.

Contrary to $\mathcal{C}^{\mathrm{Re}}_{0,1}(0)$, the contour line $\mathcal{C}^{\mathrm{Re}}_{0.2,1}(0)$ consists of infinitely many pieces. These pieces will be denoted as $\mathcal{C}^{\mathrm{Re}}_{0.2,1}(0; \pm k)$ with $k = 1, 2, 3, \ldots$, located in the upper $(+)$ and lower $(-)$ half plane, respectively. The numbering is chosen from left to right, so that $\mathcal{C}^{\mathrm{Re}}_{0.2,1}(0; \pm 1)$ separates the light grey region in the left half plane from the dark grey in the right half plane. The line $\mathcal{C}^{\mathrm{Re}}_{0.2,1}(0; +2)$ is the boundary of the light grey region surrounding the first white 'finger' (lobe) in the upper half plane, and $\mathcal{C}^{\mathrm{Re}}_{0.2,1}(0; -2)$ is its reflection on the real axis. Similarly, for $k = 3, 4, \ldots$, note that $\mathcal{C}^{\mathrm{Re}}_{0.2,1}(0; \pm 1)$ seem to encircle the central white lobe ('bubble') by going to $\pm\mathrm{i}\infty$ parallel to the imaginary axis.

With increasing α the wedge $\mathbb{W}^+(\alpha\pi/2)$ opens, the central lobe becomes smaller, the side fingers (or lobes) grow thicker and begin to extend towards the left half plane. At the same time, the contour line $\mathcal{C}^{\mathrm{Re}}_{\alpha,1}(0; \pm 1)$ moves to the left. This is illustrated in a three-dimensional plot of $\mathrm{Re}\, \mathrm{E}_{0.333,1}(z)$ in figure 5. In this figure, we have also indicated the complex zeros as the intersection of $\mathcal{C}^{\mathrm{Re}}_{0.333,1}(0)$ (shown as thick solid lines) and $\mathcal{C}^{\mathrm{Im}}_{0.333,1}(0)$ (shown as thick dashed lines). At $\alpha = 1/2$, the contours $\mathcal{C}^{\mathrm{Re}}_{0.5,1}(0; \pm 1)$ cross the imaginary axis.

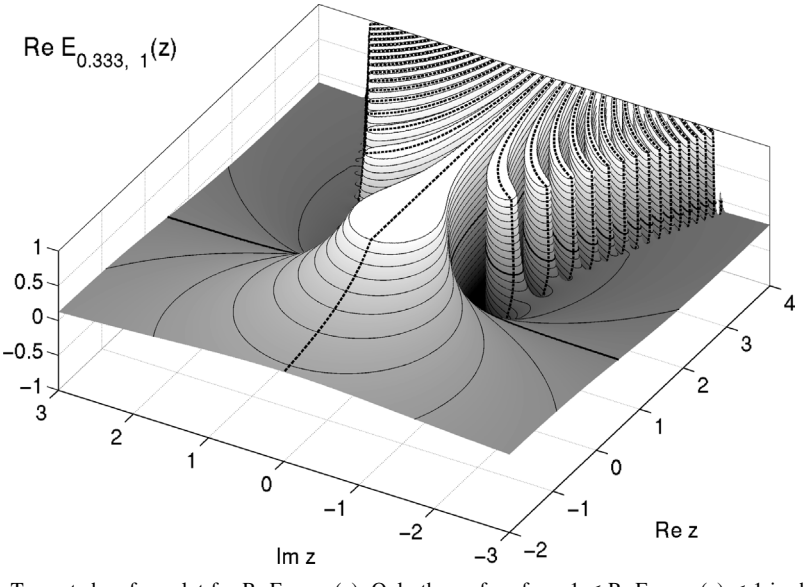

Figure 5. Truncated surface plot for $\mathrm{Re}\, \mathrm{E}_{0.333,1}(z)$. Only the surface for $-1 \leq \mathrm{Re}\, \mathrm{E}_{0.333,1}(z) \leq 1$ is shown. The contour lines $\mathcal{C}^{\mathrm{Re}}_{0.333,1}(0)$ are shown as thick solid lines. The contour lines $\mathcal{C}^{\mathrm{Im}}_{0.333,1}(0)$ are shown as thick dashed lines. Their intersections are zeros.

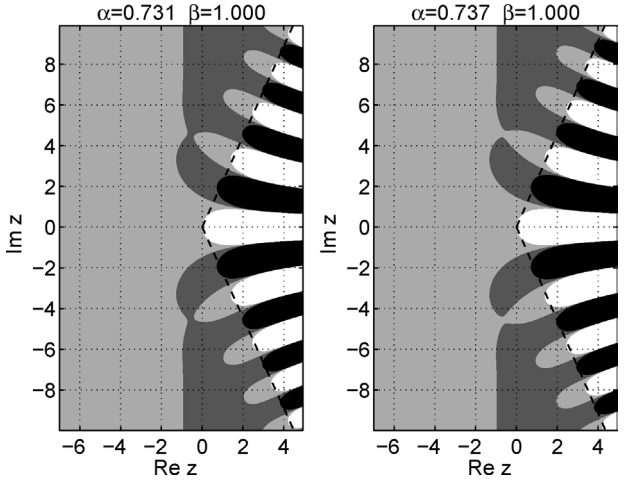

Figure 6. Contour plot for $\operatorname{Re} \mathrm{E}_{0.731,1}(z)$ and $\operatorname{Re} \mathrm{E}_{0.737,1}(z)$, before and after the first osculation estimated to occurr at $\alpha \approx 0.734375 \pm 0.000015$. The dashed lines mark the wedge $\mathbb{W}^{+}(\alpha\pi/2)$. (The grey level coding is the same as in figure 3.)

Around $\alpha \approx 0.73$, the contours $\mathcal{C}^{\mathrm{Re}}_{\alpha,1}(0; \pm 2)$ osculate the contours $\mathcal{C}^{\mathrm{Re}}_{\alpha,1}(0; \pm 1)$. The osculation eliminates a light grey finger and creates a dark grey finger. In figure 6 we show the situation before and after the osculation. This is the first of an infinity of similar osculations between $\mathcal{C}^{\mathrm{Re}}_{\alpha,1}(0; \pm 1)$ and $\mathcal{C}^{\mathrm{Re}}_{\alpha,1}(0; \pm k)$ for $k = 2, 3, 4, \ldots$. We estimate the value of α for the first osculation at $\alpha \approx 0.734375 \pm 0.000015$.

For $\alpha \to 1$, the dark grey fingers (where $\operatorname{Re} \mathrm{E}_{\alpha,\beta} < 0$) extend more and more into the left half plane. For $\alpha = 1$, the wedge $\mathbb{W}^{+}(\pi/2)$ becomes the right half plane and the lobes or fingers run parallel to the real axis. The dark grey fingers and, therefore, the oscillations, now extend to $-\infty$. The contour lines $\mathcal{C}^{\mathrm{Re}}_{1,1}(0; \pm k)$ degenerate into

$$\mathcal{C}^{\mathrm{Re}}_{1,1}(0; \pm k) = \left\{ z \in \mathbb{C} \colon \operatorname{Im} z = \pm \frac{k\pi}{2} \right\}, \quad k = 1, 2, 3, \ldots \tag{42}$$

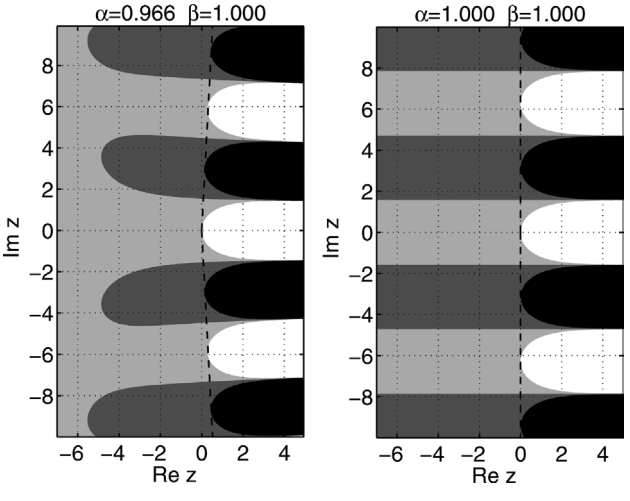

Figure 7. Contour plots for $\operatorname{Re} \mathrm{E}_{0.966,1}(z)$ and $\operatorname{Re} \mathrm{E}_{1,1}(z)$. The dashed lines mark the wedge $\mathbb{W}^{+}(\alpha\pi/2)$. (The grey level coding is the same as in figure 3.)

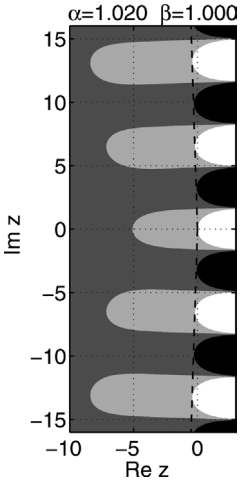

Figure 8. Contour plot for $\mathrm{Re}\,\mathrm{E}_{1.02,1}(z)$. The dashed lines mark the wedge $\mathbb{W}^{+}(\alpha\pi/2)$. (The grey level coding is the same as in figure 3.)

i.e. into the straight lines parallel to the real axis. This case is shown in figure 7. For $\alpha = 1 + \epsilon$ with $\epsilon > 0$ the grey fingers are again finite. This is shown in figure 8.

As α is increased further, the fingers grow thicker and approach each other near the negative real axis. For $\alpha \approx 1.42215 \pm 0.00005$, the first of an infinite cascade of osculations appears. This is shown in figure 9. The limit $\alpha \to 2$ is illustrated in figures 10 and 11. Note that the background colour changes from light grey in figure 10 to dark grey in figure 11 in agreement with the discussion of the complex zeros above.

For $\alpha > 2$ the behaviour changes drastically. Figure 12 shows the contour plot for $\alpha = 3, \beta = 1$. Note the scale of the axes. As a result, there are no visible dark or light grey regions. The wedge-shaped region is absent. The rays delimiting the wedge may still be viewed as if the fingers were following them in the same way as for $\alpha < 2$. Thus the fingers are more strongly bent as they approach the negative real axis.

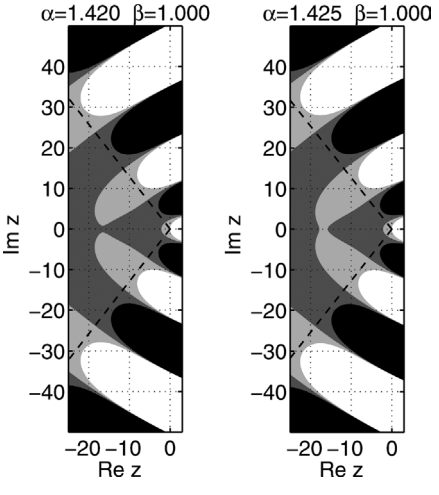

Figure 9. Contour plot for $\mathrm{Re}\,\mathrm{E}_{1.420,1}(z)$ and $\mathrm{Re}\,\mathrm{E}_{1.425,1}(z)$ before and after the osculation estimated to occurr at $\alpha \approx 1.42215 \pm 0.00005$. The dashed lines mark the wedge $\mathbb{W}^{+}(\alpha\pi/2)$. (The grey level coding is the same as in figure 3.)

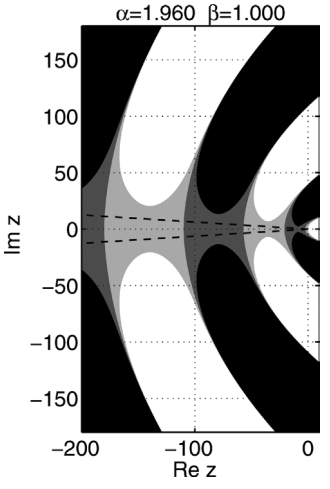

Figure 10. Contour plot for $\mathrm{Re}\,\mathrm{E}_{1.96,1}(z)$. The dashed lines mark the wedge $\mathbb{W}^{+}(\alpha\pi/2)$. (The grey level coding is the same as in figure 3.)

Now we turn to the cases $\beta \neq 1$ choosing $\alpha = 1/3$ for illustration. For $\beta > 1$, equation (41) implies that the central lobe first grows (because $\Gamma(\beta)$ diminishes) and then shrinks as $\beta \to \infty$ for small values of α. This is illustrated in the upper left subfigure of figure 13. For reference, the case $\beta = 1$ is also shown in the upper right subfigure of figure 13.

More interesting behaviour can be seen for $\beta < 1$. In this case, the contours $\mathcal{C}^{\mathrm{Re}}_{1/3,\beta}(0; \pm 1)$ stop running to infinity parallel to the imaginary axis. Instead they seem to approach infinity along the rays extending into the negative half axis as illustrated in the lower left subfigure of figure 13. At the same time, a sequence of osculations between $\mathcal{C}^{\mathrm{Re}}_{1/3,\beta}(0; \pm k)$ and $\mathcal{C}^{\mathrm{Re}}_{1/3,\beta}(0; \pm(k+1))$ begins to start from $k = \infty$. One of the last of these osculations can be seen for $\beta = 1/3$ on the lower right subfigure of figure 13. As β falls below $1/3$, the contour $\mathcal{C}^{\mathrm{Re}}_{1/3,\beta}(0; +1)$ coalesces with $\mathcal{C}^{\mathrm{Re}}_{1/3,\beta}(0; -1)$ to form a new large finite central lobe. This new second lobe becomes smaller and retracts towards the origin for $\beta \to 0$. This can be seen from

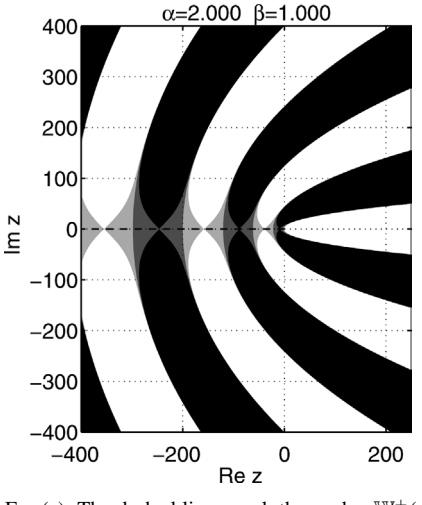

Figure 11. Contour plot for $\mathrm{Re}\,\mathrm{E}_{2,1}(z)$. The dashed lines mark the wedge $\mathbb{W}^{+}(\alpha\pi/2)$. (The grey level coding is the same as in figure 3.)

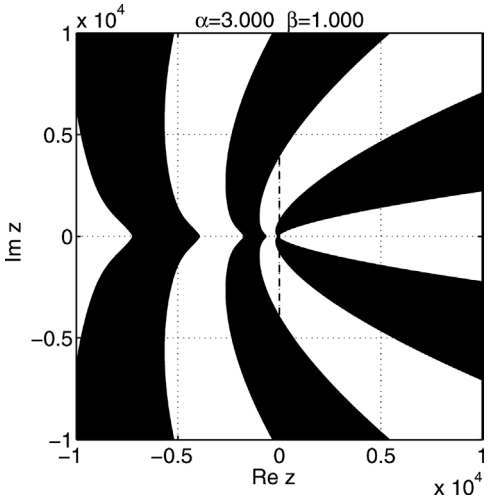

Figure 12. Contour plot for $\mathrm{Re}\,\mathrm{E}_{3,1}(z)$. The dashed lines mark the wedge $\mathbb{W}^{+}(\alpha\pi/2)$. (The grey level coding is the same as in figure 3.)

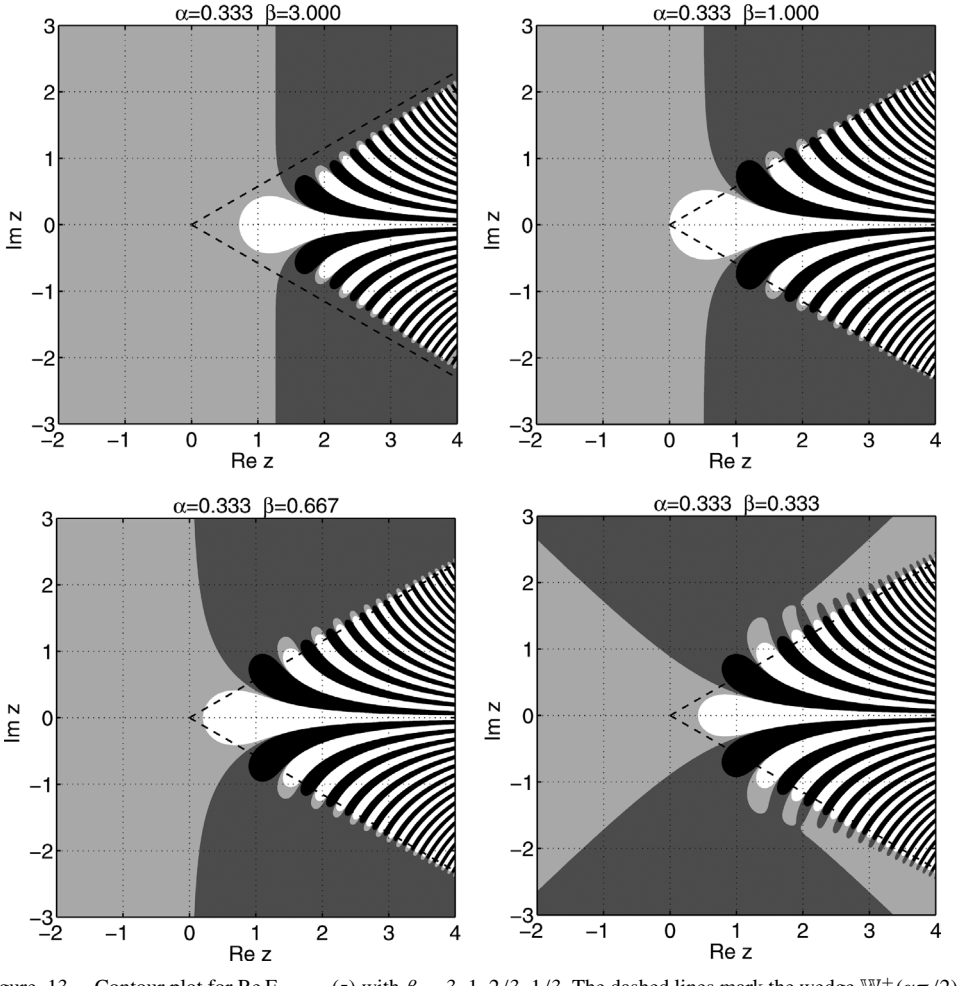

Figure 13. Contour plot for $\mathrm{Re}\,\mathrm{E}_{0.333,\beta}(z)$ with $\beta = 3, 1, 2/3, 1/3$. The dashed lines mark the wedge $\mathbb{W}^{+}(\alpha\pi/2)$. (The grey level coding is the same as in figure 3.)

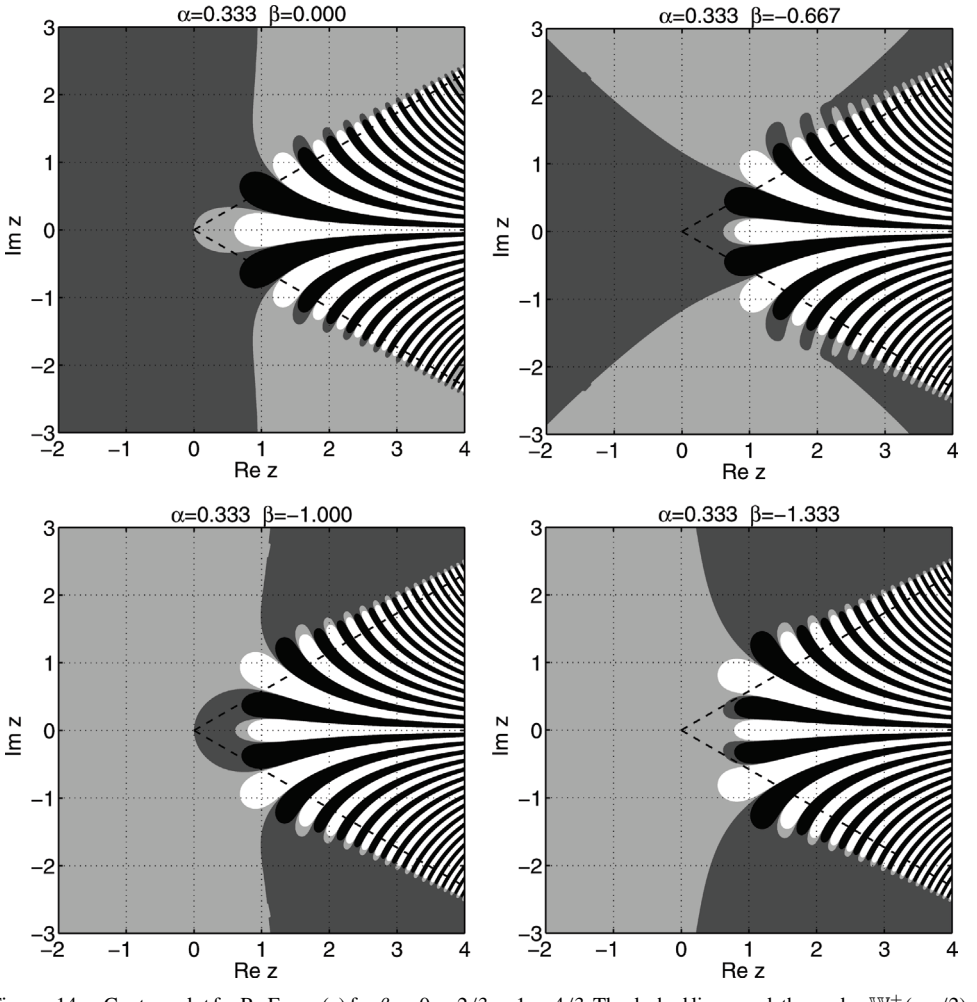

Figure 14. Contour plot for $\mathrm{Re}\,\mathrm{E}_{1/3,\beta}(z)$ for $\beta = 0, -2/3, -1, -4/3$. The dashed lines mark the wedge $\mathbb{W}^{+}(\alpha\pi/2)$. (The grey level coding is the same as in figure 3.)

the upper left subfigure of figure 14 where the case $\beta = 0$ is shown. As β falls below zero, the same process of formation of a new central lobe accompanied by a cascade of osculations starts again. This occurs iteratively whenever β crosses a negative integer, and is a consequence of the poles in $\Gamma(\beta)$.

4. Inverse Mittag-Leffler functions

We introduce the inverse generalized Mittag-Leffler function $\mathrm{L}_{\alpha,\beta}(z)$ as the solution of the equation

$$\mathrm{L}_{\alpha,\beta}(\mathrm{E}_{\alpha,\beta}(z)) = z. \tag{43}$$

Our ability to calculate $\mathrm{E}_{\alpha,\beta}(z)$ allows us to evaluate also $\mathrm{L}_{\alpha,\beta}(z)$ by solving this functional equation numerically. We have succeeded in determining the principal branch of $\mathrm{L}_{\alpha,\beta}(z)$ in such a way that three conditions are fulfilled. (1) The function $\mathrm{L}_{\alpha,\beta}(z)$ is single valued and well defined on its principal branch. (2) Its principal branch reduces to the principal branch of

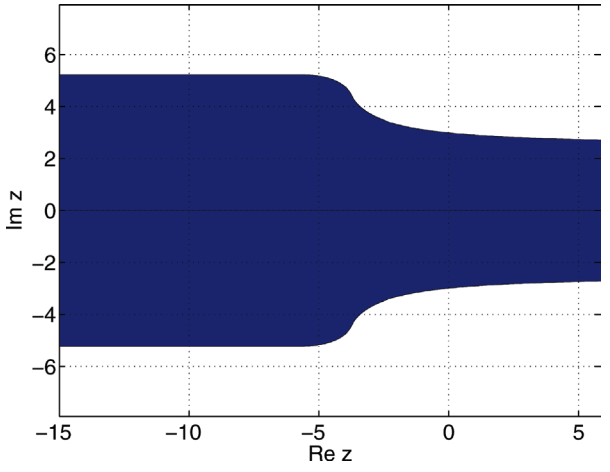

Figure 15. The dark region corresponds to the principal branch of the inverse generalized Mittag-Leffler function $L_{\alpha,\beta}(z)$ for $\alpha = 0.95$, $\beta = 1$.

the logarithm for $\alpha \to 1$. (3) Its principal branch is a simply connected subset of the complex plane. Figure 15 shows the principal branch for the case $\alpha = 0.95$, $\beta = 1$.

References

[1] Erdelyi, A. *et al.*, 1955, *Higher Transcendental Functions*, Vol. III (New York: McGraw Hill Book Co.).
[2] Mittag-Leffler, G., 1903, *Comptes Rendus de l'Academic des, Sciences Paris*, **136**, 537.
[3] Mittag-Leffler, G., 1903, *Comptes Rendus de l'Academic des, Sciences Paris*, **137**, 554.
[4] Mittag-Leffler, G., 1904, *Rendiconti della reale Accademia dei Lincei*, **13**, 3.
[5] Mittag-Leffler, G., 1905, *Acta Mathematica*, **29**, 101.
[6] Wiman, A., 1905, *Acta Mathematica*, **29**, 191.
[7] Wiman, A., 1905, *Acta Mathematica*, **29**, 217.
[8] Nigmatullin, R., 1986, *Physical. Status solidi B*, **133**, 425.
[9] Wyss, W., 1986, *Journal of Mathematical Physics*, **27**, 2782.
[10] Gaul, L., Klein, P. and Kempfle, S., 1991, *Mechanical Systems and Signal Processing*, **5**, 81.
[11] Jumarie, G., 1992, *Journal of Mathematical Physics*, **33**, 3536.
[12] Hilfer, R. and Anton, L., 1995, *Physical Review E, Rapid Communications*, **51**, R848.
[13] Hilfer, R., 1995, *Fractals*, **3**(1), 211.
[14] Hilfer, R., 1995, *Chaos, Solitons & Fractals*, **5**, 1475.
[15] Beyer, H. and Kempfle, S., 1995, *Zeitschrift fur Angewandte Mathematik und Mechanik*, **75**, 623.
[16] Schneider, W. and Wyss, W., 1989, *Journal of Mathematical Physics*, **30**, 134.
[17] Hilfer, R., 2000, *Applications of Fractional Calculus in Physics* (Singapore: World Scientific Publ. Co.).
[18] Hilfer, R., Metzler, R., Blumen, A. and Klafter, J. (Eds), 2002, *Chemical Physics*, **284**.
[19] Hilfer, R., 2003, *Physica A*, **329**, 35.
[20] Gorenflo, R., Loutchko, J. and Luchko, Y., 2002, *FCAA*, **5**, 491.
[21] Seybold, H. and Hilfer, R., 2005, to be published.
[22] Podlubny, I., 1999, *Fractional Differential Equations* (London: Academic Press).
[23] Seybold, H., 2003, Diplomarbeit, Universität Stuttgart.
[24] Wong, R. and Zhao, Y., 2002, *Constructive Approximation*, **18**, 355.